

Study of Methanol Steam Reforming and Ethanol Conversion in Conventional and Membrane Reactors

A. A. Lytkina*, A. B. Ilin, and A. B. Yaroslavtsev

Topchiev Institute of Petrochemical Synthesis, Russian Academy of Sciences, Moscow, Russia

*e-mail: lytkina@ips.ac.ru

Received April 20, 2016

Abstract—Research results for methanol steam reforming and ethanol conversion in a conventional and a membrane reactor in the presence of Ru–Rh/DND, $\text{LiZr}_2(\text{PO}_4)_3$, and $\text{Li}_{1.1}\text{Zr}_{1.9}\text{In}_{0.1}(\text{PO}_4)_3$ catalysts have been described. The samples have been characterized by X-ray diffraction, scanning electron microscopy, and the BET method. The study of the catalytic properties of the catalyst composites has shown that the Ru–Rh/DND catalyst mostly mediates the dehydrogenation process, while $\text{LiZr}_2(\text{PO}_4)_3$ and $\text{Li}_{1.1}\text{Zr}_{1.9}\text{In}_{0.1}(\text{PO}_4)_3$ exhibit activity in both the dehydration and dehydrogenation reactions. The membrane process with a Pd–Ru alloy membrane provides a 20% increase in the hydrogen yield.

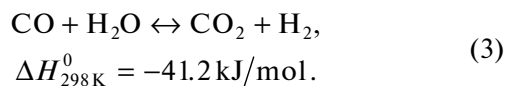
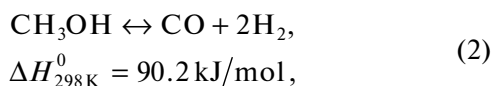
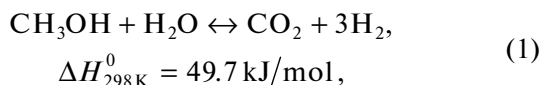
Keywords: membrane catalysis, NASICON, methanol steam reforming, ethanol conversion

DOI: 10.1134/S0965544116110104

INTRODUCTION

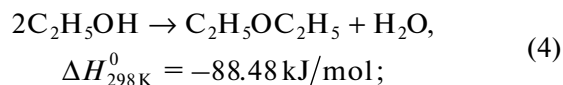
Aggravated environmental problems have raised interest in the use of renewable raw materials, promising types of which are biomass and bioalcohols resulting from the primary processing of biomass (methanol, ethanol). Bioalcohols can be used as precursors for producing hydrogen or a number of valuable products, such as hydrocarbons, ethers, aldehydes, ketones, hydrogen, etc. [1]. The reforming of alcohols whose molecules are much more reactive than methane molecules occurs at low temperatures [2–6].

In addition to target reaction (1), methanol steam reforming (MSR) is characterized by the occurrence by methanol decomposition (2) and reaction of the produced CO with water (3):

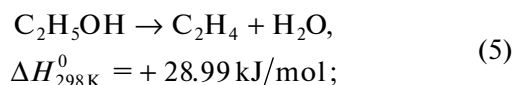


Ethanol conversion products can be much more diverse. Ethanol conversion can occur via a few alternative pathways:

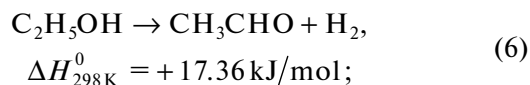
dehydration to diethyl ether (DEE):



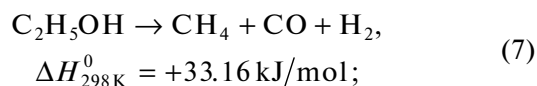
dehydration to ethylene:



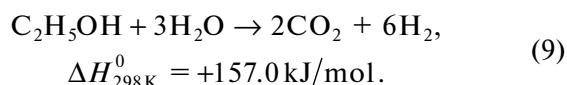
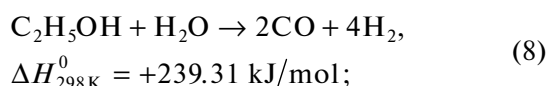
dehydration to acetaldehyde:



methanation:



and steam reforming:



In addition, the dehydrogenation of the reaction products and catalytic crosslinking can occur to form valuable extended-chain hydrocarbons. Depending on the target product, catalysts with different structures and compositions are used for alcohol conversion.

Typically, hydrogen is produced using metal catalysts supported on various supports. It was shown that noble metals, such as Rh, Ir, Pt, Ru, and Pd, exhibit high activity in alcohol reforming [7]. Furthermore, Rh is regarded as one of the most active metals in the series of noble metals [8]. The authors of [9–13] also consider Ru as a promising catalyst for steam reforming and oxidative steam reforming. Since the use of noble metals in catalysis is limited to their high cost [14], of considerable interest are catalysts with a low content of noble metals [15] and materials composed of a few metals [15–17].

An important problem is the improvement of the selectivity and coking resistance of the composite. In this respect, novel carbon materials, such as nanotubes, graphene, and detonation nanodiamonds (DNDs), are attracting close attention; the unique properties of these materials make them suitable for use as catalyst supports [6, 18, 19]. DND nanoparticles consist of a core with a diamond lattice and an amorphous carbon shell. In addition, the DND surface contains a large amount of oxygen-containing functional groups that provide high adsorption properties of this material [20].

A promising type of alcohol conversion catalysts are complex phosphates [21, 22]. Materials with a NASICON-type (NA Super Ionic CONductor) structure are compounds with a general formula of $A_xB_2(ZO_4)_3$, where A is typically an alkali or alkaline earth element, B is a polyvalent element (Zr, Ti, Sc, etc.), and Z is phosphorus or silicon. Their structure is composed of edge-linked BO_6 octahedra and ZO_4 tetrahedra. The voids of the framework formed by them are occupied by the A cations [23–30].

Heterovalent substitution provides variation in the number and strength of acid (Lewis and Brønsted) and redox surface sites. The chemical and thermal resistance of catalysts based on these compounds makes them suitable for use under conditions where metal catalysts undergo degradation.

One of the products of the above processes is hydrogen. A catalytic process version is membrane catalysis, in which some of the products are selectively separated or fed to the reaction mixture through a membrane [5, 31–33]. In particular, the problem of producing high-purity hydrogen can be effectively solved using membrane catalysis owing to the selective removal of hydrogen across a Pd-containing membrane [34–36]. Other advantages of this method are the possibility of shifting the thermodynamic equilibrium owing to the removal of the product. Therefore, even if hydrogen is not the main product, the removal of it can significantly change the process direction and the product yield [5]. Compared with pure Pd membranes, membranes made of some Pd alloys have a number of advantages because they exhibit a higher hydrogen permeability, strength, thermal stability, and catalytic activity [37–41]. The alloying of Pd with Ru

(even in small amounts of ~1 wt %) leads to an increase in the mechanical stability of the membrane during thermal cycling in hydrogen [42].

The aim of this study was to examine the MSR and ethanol conversion processes implemented by membrane catalysis. Of particular interest was to compare the two processes; in one of them, hydrogen is the main product, while in the other, the hydrogen yield is low; however, the use of membrane catalysis makes it possible to change the ratio of the conversion products.

EXPERIMENTAL

Catalyst Synthesis, Physicochemical Investigation, and Catalytic Test Procedures

The Ru–Rh/DND catalyst was prepared by the reduction of metal precursors (ruthenium(III) chloride and rhodium(III) chloride) at room temperature in a liquid phase using 0.5 M $NaBH_4$ as a reducing agent. The amount of the precursor was calculated according to the total metal content in the material after complete reduction (7.5 wt %) and an atomic ratio of 1 : 1. The synthesized catalyst was exposed to a H_2 (5%)/Ar atmosphere (20 mL/min) at 350°C for 3 h to reduce the metals.

The $LiZr_2(PO_4)$ and $Li_{1 \pm 0.1}Zr_{1.9}In_{0.1}(PO_4)$ compounds were synthesized by the Pechini method [43–45]. To this end, $ZrOCl_2 \times 8 H_2O$, citric acid, Li_2CO_3 , and $NH_4H_2PO_4$ were sequentially dissolved in a deionized water–ethylene glycol mixture (10 : 2 mL/mL); after that, the solution pH was rapidly adjusted to 5.5 by the addition of an ammonia solution. The resulting solution was sequentially subjected to heat treatments at 95°C (24 h), 150°C (24 h), 350°C (4 h), and 750°C (10 h). To prepare LZInP, a weighed portion of In_2O_3 was dissolved in a minimum amount of hot concentrated nitric acid and added to the mixture.

The surface area and pore size of the synthesized catalysts were examined by the BET method on an ASAP-2020N instrument (Micromeritics, United States). X-ray diffraction (XRD) analysis of the samples was conducted using a Rigaku D/Max-2200 X-ray diffractometer ($CuK_{\alpha 1}$ radiation). Spectrum processing and qualitative analysis were conducted using the Rigaku Application Data Processing software package. Particle size (coherent scattering region (CSR)) was determined from the XRD peak widths using the Scherrer formula

$$d = \frac{k\lambda}{(B - b) \cos \theta}, \quad (10)$$

where $k = 0.89$ is the Scherrer constant, $\lambda = 1.5406 \text{ \AA}$ is the wavelength of the radiation used, B is the peak

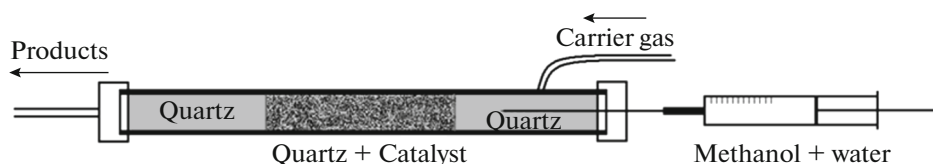


Fig. 1. Diagram of a conventional flow reactor.

half-width at half-maximum (2θ), b is the instrumental broadening (2θ), and θ is the peak position angle.

Transmission electron microscopy (TEM) images were recorded on a JEM 2100 transmission electron microscope at an accelerating voltage of 200 kV and a point resolution of 0.23 nm. Micrographs of the samples were recorded using a Carl Zeiss NVision 40 scanning electron microscope (SEM) equipped with an electron probe microanalysis attachment. The accelerating voltage was 1 kV.

MSR and catalytic conversion of ethanol were conducted in a conventional stainless steel tubular flow reactor (Fig. 1). Reaction products were analyzed on LHM 8MD (phase, Porapak T; carrier gas, He); Chrom-4 (phase, CaA Zeosorb; carrier gas, Ar); and Kristallyuks 4000M chromatographs (phase, HayeSep T 60/80 mesh, SKT-6; carrier gas, He and phase, Mole Seive 5 A; carrier gas, Ar); in the all cases, a thermal conductivity detector was used.

The catalyst with a weight of with 0.3 g was mixed with quartz granules and placed at the center of the reactor. Before each set of experiments, the metal catalyst was in situ reduced with an H_2 (5%)/Ar mixture (20 mL/min) at a temperature of 350°C for 3 h. The carrier gas was Ar or He (20 mL/min). For steam reforming, a liquid mixture of methanol and water in a molar ratio of 1: 1 was fed into an evaporator using an Instilar1488 Dixion infusion pump at a flow rate of 2 mL/h and then mixed with the carrier gas stream. To study the catalytic conversion, ethanol was fed into the reactor by passing the carrier gas through a bubbler thermostated at 11°C.

The MSR and ethanol conversion reactions were also run in a membrane reactor. Catalyst samples (0.3-g load) mixed with quartz granules (1–3 mm fraction) were placed in the reaction zone of a membrane reactor, which is schematically shown in Fig. 2. The reactor consisted of two stainless steel cylindrical compartments separated by a dense membrane of a Pd–Ru alloy (6 wt % Ru). The studied membranes had thicknesses of 12 and 70 μm . The reactor was sealed using two gaskets made of copper and Graphlex. The flow rate of the purge gas—argon—on the permeate and retentate side was 20 cm^3/min . Reaction products were analyzed by the method described above.

Degree of conversion of alcohol X (mol %) was calculated according to the analysis results using the following equation:

$$X = (\varphi_0 - \varphi_1) / \varphi_0 \times 100,$$

where φ_0 and φ_1 are the initial and final concentrations of methanol, respectively.

RESULTS AND DISCUSSION

Catalyst and Substrate Structural and Morphological Characteristics

The X-ray diffraction patterns of the Ru–Rh/DND catalyst show broad peaks with maxima at 43.6° corresponding to the DND (Fig. 3a). The narrower peaks are attributed to the Ru–Rh alloy for which the reflection peaks are located between the positions characteristic of the individual metals. The unit cell parameter of the resulting alloy is 0.38044 ± 0.0002 nm.

The XRD data for lithium zirconium phosphates showed that the $\text{LiZr}_2(\text{PO}_4)_3$ and $\text{Li}_{1.1}\text{Zr}_{1.9}\text{In}_{0.1}(\text{PO}_4)_3$ samples are composed of a single phase and correspond to the monoclinic NASICON modification (Fig. 3b).

According to SEM, the Ru–Rh/DND samples are framework agglomerates with a size of 50–300 nm, which are composed of significantly smaller particles (Fig. 4a). TEM data provide more information about these materials. The data show that the average particle size of the metals in the studied composite is 5–8 nm (Fig. 5). The particle size of the catalysts with a NASICON structure varies in a range of 50–200 nm (Fig. 4b).

The table lists the specific surface areas of the synthesized catalysts and the average particle size of the composites determined by the BET method and calculated according to the XRD pattern linewidths (CSRs). The surface area of the Ru–Rh/DND sample is determined by the degree of dispersion of the DND because the content of DND in the composite is considerably higher than that of the metals and the XRD pattern lines corresponding to the Ru–Rh alloy are significantly narrower, thereby indicating that the particle size of this material is larger.

The specific surface areas of the catalysts based on lithium zirconium phosphates vary in a range of

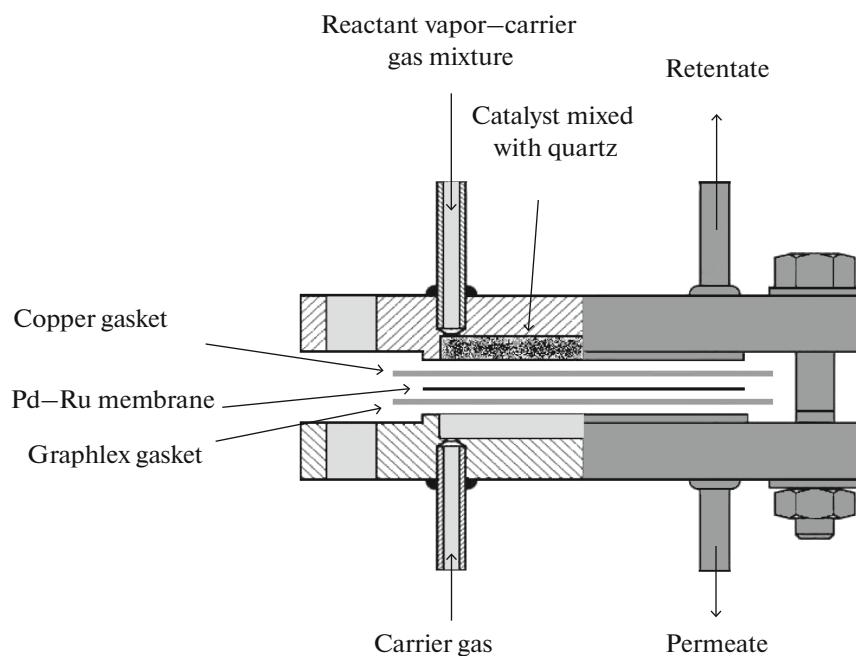


Fig. 2. Diagram of a membrane reactor.

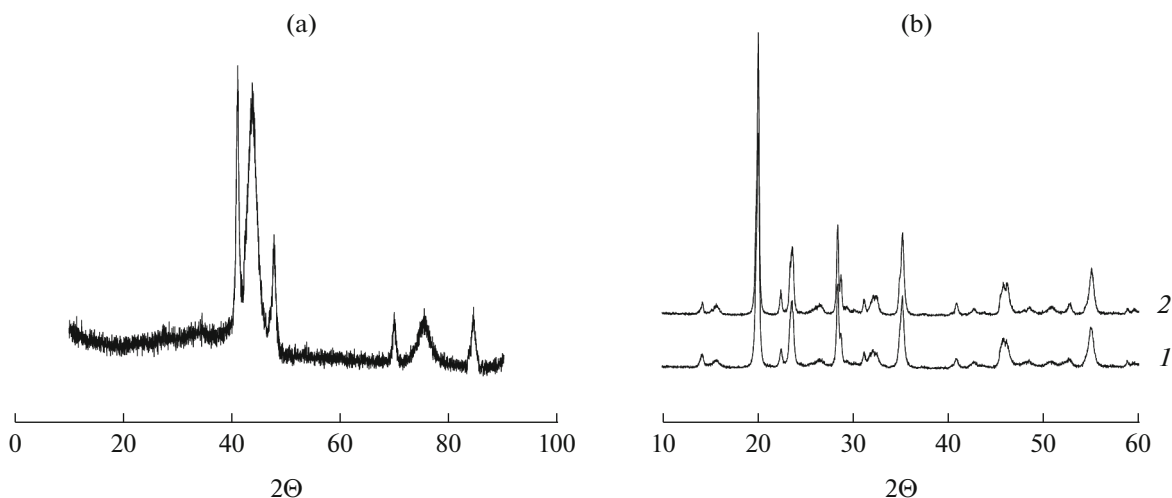


Fig. 3. (a) XRD patterns of the Ru-Rh/DND catalyst and (b) XRD patterns of (1) the $\text{LiZr}_2(\text{PO}_4)_3$ and (2) $\text{Li}_{1.1}\text{Zr}_{1.9}\text{In}_{0.1}(\text{PO}_4)_3$ catalysts.

11–16 m^2/g (see table). The average particle sizes calculated from the BET data are 2—and more—times higher than the values determined by calculating the

CSR (table). This fact, along with the SEM data, suggests that a significant portion of the particles are aggregated.

Specific surface area and characteristic particle size of the test catalysts, as calculated by different methods

Catalyst	Specific surface area, m^2/g	CSR size, nm	Average particle size determined from surface area, nm
Ru-Rh/DND	289 ± 3	13 ± 1	20
$\text{LiZr}_2(\text{PO}_4)_3$	16 ± 1	49.4 ± 2.5	87
$\text{Li}_{1.1}\text{Zr}_{1.9}\text{In}_{0.1}(\text{PO}_4)_3$	11 ± 1	81.0 ± 4.0	170

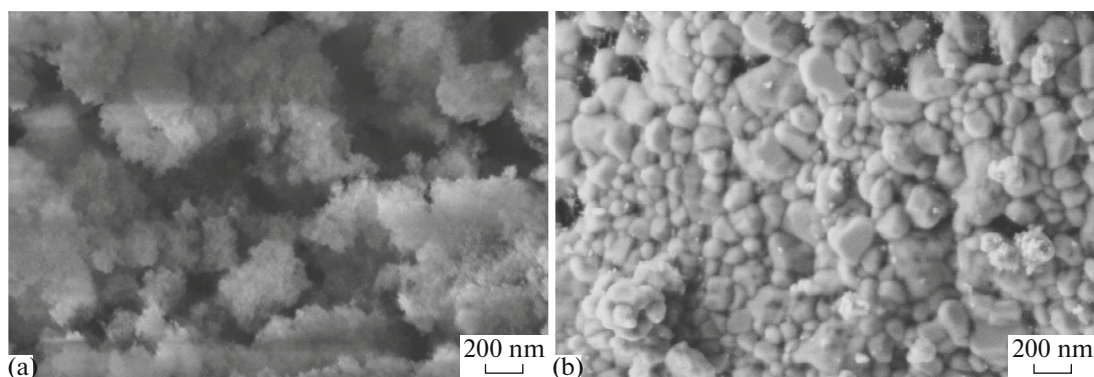


Fig. 4. SEM micrographs of (a) the Ru–Rh/DND and (b) $\text{Li}_{0.9}\text{Zr}_{1.8}\text{In}_{0.1}\text{Nb}_{0.1}\text{P}_{2.9}\text{Mo}_{0.1}\text{O}_{12}$ samples.

Catalyst Activity in Dehydrogenation and Dehydration Reactions

Conventional flow reactor. A comparative study of the catalytic activity of the synthesized samples in the dehydration and dehydrogenation of C_1 – C_2 alcohols in a conventional flow reactor was conducted.

A distinctive feature of DNDs is a high concentration of oxygen-containing groups on their surface [20].

According to the derived values, the degree of conversion of methanol over the Ru–Rh/DND catalyst was 85% at 300°C. With a further increase in temperature, the degree of conversion did not increase; however, the process became less selective for hydrogen.

Figure 6 shows the temperature dependences of the amounts of hydrogen and carbon monoxide produced over the Ru–Rh/DND catalyst. At 330–350°C, the hydrogen flux corresponds to a yield of 2.3 mol of hydrogen per mole of fed alcohol, while the theoretically possible value is 3 mol/mol. At high temperatures, in addition to the target reaction, methanol undergoes decomposition by reaction (6), which leads

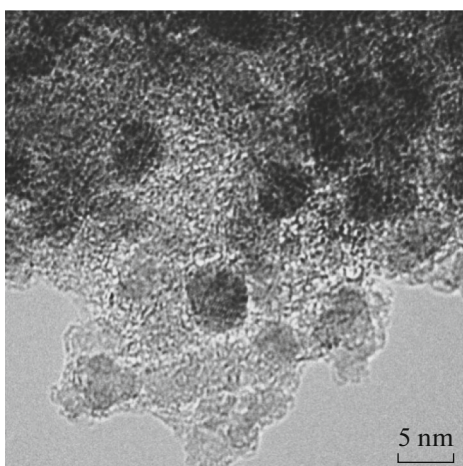


Fig. 5. TEM micrograph of the Ru–Rh/DND sample.

to the appearance of about 3 vol % of a CO impurity in the resulting hydrogen (Fig. 6, curve 2).

The $\text{LiZr}_2(\text{PO}_4)_3$ and $\text{Li}_{1.1}\text{Zr}_{1.9}\text{In}_{0.1}(\text{PO}_4)_3$ samples were used as ethanol conversion catalysts; they exhibited activity in both the dehydration and dehydrogenation of ethanol. This feature provides the occurrence of ethanol conversion via a few alternative pathways: dehydration to DEE, dehydration to ethylene, dehydrogenation to acetaldehyde, methanation, and steam reforming. Other possible reactions are the dehydrogenation of the reaction products and the catalytic crosslinking of the resulting unsaturated hydrocarbons.

In the case of the studied catalysts, the main products of the processes are acetaldehyde, hydrogen, DEE, C_2 hydrocarbons (ethylene and ethane produced in the hydrogenation of ethylene by hydrogen during reaction), and C_4 hydrocarbons. The formation of CO, CO_2 , and CH_4 is also observed; however, the

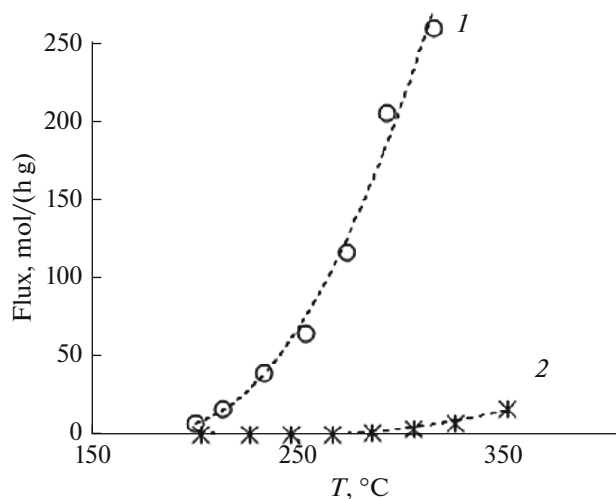


Fig. 6. Flux of (1) hydrogen and (2) CO in the presence of the Ru–Rh/DND catalyst.

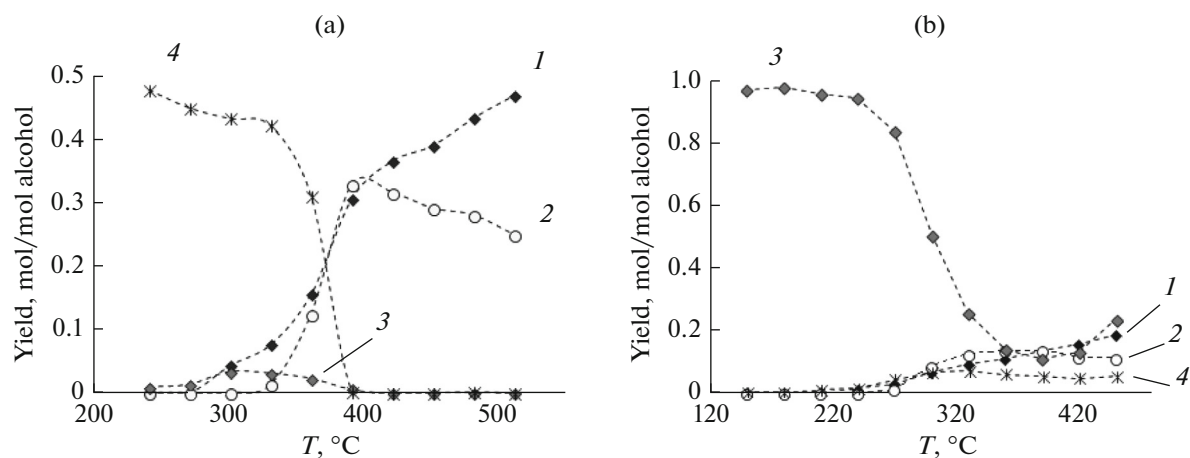


Fig. 7. Yield of (1) C_2 hydrocarbons, (2) C_4 hydrocarbons, (3) acetaldehyde, and (4) DEE in the presence of (a) the $LiZr_2(PO_4)_3$ and (b) $Li_{1.1}Zr_{1.9}In_{0.1}(PO_4)_3$ catalysts.

amounts of these products are negligible compared with the main products.

The $LiZr_2(PO_4)_3$ sample exhibits activity in the formation of C_2 and C_4 hydrocarbons and DEE. Only small amounts of acetaldehyde and hydrogen are formed; this finding suggests that ethanol dehydration reactions (4) and (5) are dominant reactions (Fig. 7).

The doping of lithium zirconium phosphate with indium leads to a decrease in the acidity of the active sites of the catalyst, which in turn leads to the inhibition of the dehydration function and an increase in the hydrogen yield (Fig. 8). With an increase in temperature, the amount of acetaldehyde decreases apparently because it is converted to hydrogen, methane, and carbon oxides.

Membrane reactor. Figure 9 shows the temperature dependences of the hydrogen flow rate in the presence of the Ru–Rh/DND and $Li_{1.1}Zr_{1.9}In_{0.1}(PO_4)_3$ catalysts. At high temperatures, for both catalysts, the hydrogen yield in the membrane reactor was 20% higher than that in the conventional flow reactor. The

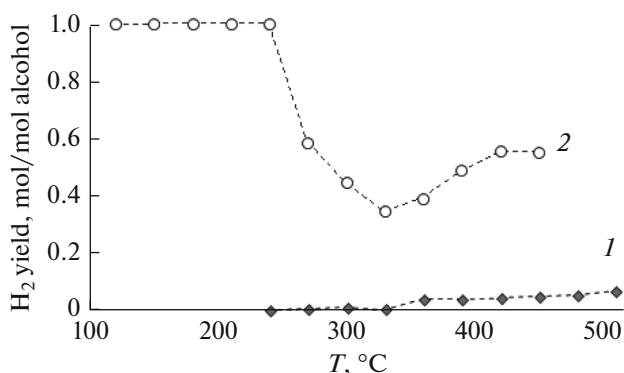


Fig. 8. Hydrogen yield in the presence of (a) the $LiZr_2(PO_4)_3$ and (b) $Li_{1.1}Zr_{1.9}In_{0.1}(PO_4)_3$ catalysts.

selective recovery of the reaction product—hydrogen—from the retentate zone leads to a shift of the equilibrium position of the hydrogen-producing reactions toward the products and to an increase in the degree of conversion of the alcohol.

For lithium zirconium phosphate, the average degree of recovery of hydrogen was 35%; in the case of the Ru–Rh/DND catalyst, this parameter did not exceed 15% (Fig. 9a). This difference can be attributed to the fact that the Ru–Rh catalyst provides high hydrogen fluxes, which lead to a significant increase in the total flow rate of the reaction products along the membrane and a change in the macrokinetics. Note that the permeated hydrogen did not contain CO or other impurities.

In the case of MSR over the Ru–Rh/DND composite in the membrane reactor, the process selectivity for hydrogen also increased. The amount of carbon monoxide produced in the conventional reactor was about 3% at a temperature of $\sim 330^\circ C$. In the membrane reactor, this parameter decreased to 1%.

In addition, an increase in the degree of conversion of ethanol and in the activity in the formation of acetaldehyde is observed in the presence of the $Li_{1.1}Zr_{1.9}In_{0.1}(PO_4)_3$ catalyst (Fig. 10). These effects are attributed to a shift of the thermodynamic equilibrium caused by the removal of hydrogen through the membrane; the shift contributes to the intensification of the hydrogen-producing reactions.

CONCLUSIONS

A comparative study of the MSR and ethanol conversion processes by conventional and membrane catalysis has been conducted.

For the Ru–Rh/DND catalyst, hydrogen is the main product. At $330\text{--}350^\circ C$, the hydrogen flux corresponds to a yield of 2.3 mol of hydrogen per mole of

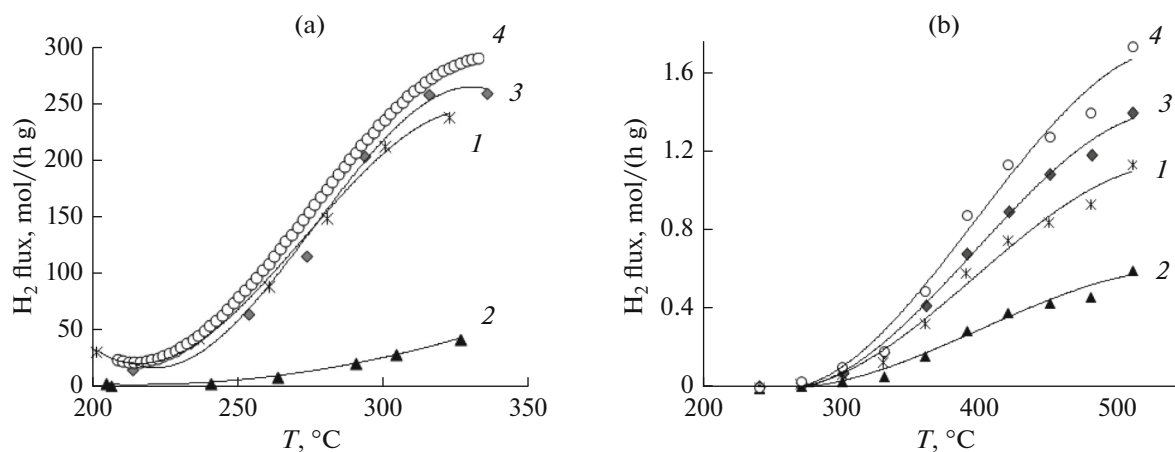


Fig. 9. Hydrogen flow rates in (1) the retentate and (2) permeate zones, and (3) conventional reactor and (4) the total flux of hydrogen in the membrane reactor in the presence of (a) the Ru–Rh/DND and (b) Li_{1.1}Zr_{1.9}In_{0.1}(PO₄)₃ catalysts.

fed alcohol, while the theoretically possible value is 3 mol/mol. At high temperatures, a CO impurity in the amount of 3 vol % is observed in the resulting hydrogen.

The LiZr₂(PO₄)₃ sample exhibits activity in the formation of C₂ and C₄ hydrocarbons and DEE. Only small amounts of acetaldehyde and hydrogen are formed; this finding suggests that ethanol undergoes conversion mostly through dehydration reactions. The doping of lithium zirconium phosphate with indium leads to a decrease in the acidity of the active sites of the catalyst, which in turn leads to the inhibition of the dehydration function and an increase in the hydrogen yield.

At high temperatures, for both catalysts, the hydrogen yield in the membrane reactor is 20% higher than that in the conventional flow reactor. In the case of the Ru–Rh/DND composite, the selective recovery of

hydrogen from the retentate zone leads to an increase in the MSR selectivity for hydrogen and a decrease in the formation of CO. In the presence of Li_{1.1}Zr_{1.9}In_{0.1}(PO₄)₃, the degree of conversion of ethanol and the acetaldehyde yield increase owing to a shift of the thermodynamic equilibrium. Hydrogen in the permeate zone does not contain CO or other impurities.

ACKNOWLEDGMENTS

This work was supported by the Ministry of Education and Science of the Russian Federation, agreement no. 14.607.21.0033.

REFERENCES

1. F. Frusteri and G. Bonura, *Compendium of Hydrogen Energy*, vol. 1: *Hydrogen Production and Purification*, Ed. by V. Subramani, A. Basile, and T. N. Veziroğlu, No. 83 of *Woodhead Publishing Series in Energy* (Elsevier, Amsterdam, 2015), p. 109.
2. A. B. Yaroslavtsev, Yu. A. Dobrovolskii, N. S. Shaglaeva, et al., *Usp. Khim.* **81**, 191 (2012).
3. O. G. Ellert, M. V. Tsodikov, S. A. Nikolaev, and V. M. Novotortsev, *Usp. Khim.* **83**, 718 (2014).
4. L. L. Makarshin and V. N. Parmon, *Russ. Khim. Zh.* **50**, 19 (2006).
5. N. L. Basov, M. M. Ermilova, N. V. Orekhova, and A. B. Yaroslavtsev, *Usp. Khim.* **82**, 352–368 (2013).
6. E. Yu. Mironova, M. M. Ermilova, N. V. Orekhova, et al., *Catal. Today* **236**, 64 (2014).
7. D. R. Palo, A. D. Dagle, and J. D. Holladay, *Chem. Rev.* **107**, 3992 (2007).
8. M. Krumpelt, T. Krause, J. Carter, et al., *Catal. Today* **77**, 3 (2002).
9. A. Iulianelli, T. Longo, S. Liguori, et al., *Int. J. Hydrogen Energy*, **34**, 8558 (2009).

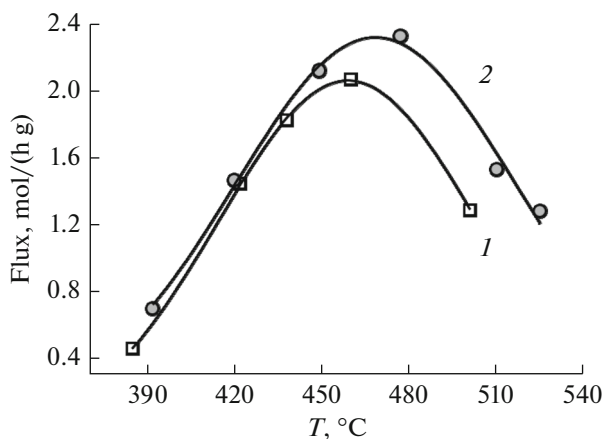


Fig. 10. Flux of acetaldehyde in (1) the conventional and (2) membrane reactors.

10. M. A. Soria, C. Mateos-Pedrero, A. Guerrero-Ruiz, and I. Rodríguez-Ramos, *Int. J. Hydrogen Energy* **36**, 15212 (2011).
11. C. C. Hung, S. L. Chen, Y. K. Liao, et al., *Int. J. Hydrogen Energy* **37**, 4955 (2012).
12. I. A. Carbajal Ramos, T. Montini, B. Lorenzut, et al., *Catal. Today* **180**, 96 (2012).
13. U. Amjad, A. Vita, C. Galletti, et al., *Ind. Eng. Chem. Res.* **52**, 15428 (2013).
14. N. Srisiriwat, S. Therdthianwong, and A. Therdthianwong, *Int. J. Hydrogen Energy* **34**, 2224 (2009).
15. S. Cavallaro, V. Chiodo, A. Vita, and S. Freni, *J. Power Sources* **123**, 10 (2003).
16. E. Vesseli, G. Comelli, R. Rosei, et al., *Appl. Catal., A* **281**, 139 (2005).
17. J. L. Bi, Y. Y. Hong, C. C. Lee, et al., *Catal. Today* **129**, 322 (2007).
18. N. N. Vershinin, O. N. Efimov, V. A. Bakaev, et al., *Fullerenes, Nanotubes, Carbon Nanostruct.* **19**, 63 (2011).
19. X. Sun, R. Wang, and D. Su, *Chin. J. Catal.* **34**, 508 (2013).
20. I. I. Kulakova, *Phys. Solid State* **46**, 636 (2004).
21. M. A. Aramendia, V. Borau, J. M. Marinas, and F. J. Romero, *Chem. Lett.*, 1361 (1994).
22. A. B. Il'in, M. M. Ermilova, N. V. Orekhova, and A. B. Yaroslavtsev, *Inorg. Mater.* **51**, 711 (2015).
23. L. O. Hagman and P. Kierkegaard, *Acta Chem. Scand.* **22**, 1822 (1968).
24. H. Kohhler and H. Schulz, *Mater. Res. Bull.* **20**, 1461 (1985).
25. A. Serghini, R. Brochu, M. Ziyad, and J. J. Vadrine, *J. Chem. Soc., Faraday Trans.* **87**, 2487 (1991).
26. Y. Brik, M. Kacimi, F. Bozon-Verduraz, and M. Ziyad, *Microporous Mesoporous Mater.* **43**, 103 (2001).
27. A. B. Il'in, S. A. Novikova, M. V. Sukhanov, et al., *Inorg. Mater.* **48**, 397 (2012).
28. E. I. Povarova, A. I. Pylinina, and I. I. Mikhaleiko, *Russ. J. Phys. Chem. A* **86**, 935 (2012).
29. A. I. Pylinina and I. I. Mikhaleiko, *Mendeleev Commun.* **22**, 150 (2012).
30. A. I. Pylinina and I. I. Mikhaleiko, *Russ. J. Phys. Chem. A* **87**, 372 (2013).
31. I. F. J. Vankelecom, K. A. L. Verwey, P. E. Neys, et al., *Top. Catal.* **5**, 125 (1998).
32. V. Diakov and A. Varma, *Chem. Eng. Sci.* **57**, 1099 (2002).
33. R. Tesser, M. D. Serio, and E. Santacesaria, *Catal. Today* **77**, 325 (2003).
34. A. Iulianelli, P. Ribeiro, A. Mendes, and A. Basile, *Renew. Sust. Energy Rev.* **24**, 355 (2014).
35. A. Iulianelli and A. Basile, *Catal. Sci. Technol.* **1**, 366 (2011).
36. E. Yu. Mironova, A. A. Lytkina, M. M. Ermilova, et al., *Int. J. Hydrogen Energy* **40**, 3557 (2015).
37. F. A. Lewis, *Platinum Met. Rev.* **26**, 121 (1982).
38. N. A. Al-Mufachi, N. V. Rees, and R. Steinberger-Wilkens, *Renew. Sust. Energy Rev.* **47**, 540 (2015).
39. H. W. Abu El Hawa, S. N. Paglieri, et al., *J. Membr. Sci.* **466**, 151 (2014).
40. V. M. Gryaznov, M. M. Ermilova, N. V. Orekhova, and G. F. Tereschenko, *Structured Catalysts and Reactors*, 2nd Ed., Ed. by A. Cybulski and J. A. Moulijn (Taylor and Francis, London, 2005), p. 579.
41. M. Itoh, M. Saito, C. Yu Li, et al., *Chem. Lett.* **34**, 1104 (2005).
42. V. M. Gryaznov, A. P. Mishchenko, V. P. Polyakova, *Dokl. Akad. Nauk SSSR* **211**, 624 (1973).
43. M. P. Pechini, US Patent, No. 3 330 697 (1967); M. Kakihana and M. Yoshimura, *Bull. Chem. Soc. Jpn.* **72**, 1427 (1999).
44. C. R. Mariappan, C. Galven, M. P. Crosnier-Lopez, et al., *Solid State Chem.* **179**, 450 (2006).
45. F. Ejehi, S. P. H. Marashi, M. R. Ghaani, and D. F. Haghshenas, *Ceram. Int.* **38**, 6857 (2012).

Translated by M. Timoshinina